Available online at www.sciencedirect.com
SCIENCE DIRECT
Journal of Solid State Chemistry 179 (2006) 1506–1512
JOURNAL OF SOLID STATE CHEMISTRY
www.elsevier.com/locate/jssc

Structure and physical properties of nonstoichiometric rare-earth cadmium antimonides, $RECd_{1-x}Sb_2$ (RE = La, Ce, Pr, Nd, Sm)

Andriy V. Tkachuk, Oksana Ya. Zelinska, Arthur Mar*

Department of Chemistry, University of Alberta, Edmonton, Alberta, Canada T6G 2G2

Received 19 October 2005; received in revised form 26 January 2006; accepted 28 January 2006
Available online 6 March 2006

Abstract

The ternary rare-earth cadmium antimonides $RECd_{1-x}Sb_2$ (RE = La, Ce, Pr, Nd, Sm) were prepared by reaction of the elements at 1000 °C. The presence of Cd defects, previously found for $LaCd_{0.700(5)}Sb_2$ and $CeCd_{0.660(4)}Sb_2$, has been confirmed by single-crystal X-ray diffraction studies for the isotypic compounds $PrCd_{0.665(3)}Sb_2$ (a = 4.3592(3) Å, c = 10.8619(7) Å), $NdCd_{0.659(3)}Sb_2$ (a = 4.3456(4) Å, c = 10.8372(9) Å), and $SmCd_{0.648(3)}Sb_2$ (a = 4.3185(4) Å, c = 10.7843(11) Å). These compounds adopt the $HfCuSi_2$-type structure (Pearson symbol $tP8$, space group $P4/nmm$, Z = 2). The electrical and magnetic properties of samples with nominal composition $RECd_{0.7}Sb_2$ were investigated. All exhibit metallic behaviour, but $CeCd_{0.7}Sb_2$ undergoes an abrupt drop in its electrical resistivity below 3 K. $LaCd_{0.7}Sb_2$ exhibits temperature-independent Pauli paramagnetism and $SmCd_{0.7}Sb_2$ displays van Vleck paramagnetism. The remaining compounds obey the modified Curie–Weiss law at high temperatures. $CeCd_{0.7}Sb_2$ undergoes ferromagnetic ordering below 3 K, reaching a saturation magnetization of ~1.0 μ_B, whereas $PrCd_{0.7}Sb_2$ and $NdCd_{0.7}Sb_2$ remain paramagnetic down to 2 K.

Keywords: Antimonide; Crystal structure; Magnetic properties; Transport properties

1. Introduction

Among the growing number of ternary rare-earth (RE) transition-metal antimonides, an especially prevalent series with the composition $REM_{1-x}Sb_2$ is formed for many late transition metals (M = Mn, Fe, Co, Ni, Pd, Cu, Ag, Au, Zn, Cd) [1–12]. They adopt the tetragonal $HfCuSi_2$-type structure (Pearson symbol $tP8$), but in most cases, this has been determined only by powder X-ray diffraction data. Although a few of these compounds are fully stoichiometric, such as $REAgSb_2$ [5,6], most are expected to exhibit some degree of partial occupancy of the transition-metal site. The definitive composition is best established by single-crystal X-ray diffraction studies. For those cases where M is assumed to be dipositive, the nonstoichiometry can be rationalized through arguments based on simple electron counting [8], in which charge balance can only be maintained through the presence of vacancies, resulting in the ideal formulation $(RE^{3+})(M^{2+})_{0.5}(Sb1)^{1-}(Sb2)^{3-}$. For example, the formula for $LaZn_{0.52}Sb_2$ appears to be correctly explained by this model [2]. More frequently, however, the compositions deviate significantly from this model, such as in $LaMn_{0.65-0.76}Sb_2$ [8] or $YNi_{0.57}Sb_2$ [12], but the reasons are unclear.

These $REM_{1-x}Sb_2$ compounds have elicited particular interest for their magnetic and transport properties, which have been measured for some of these members (M = Mn, Ni, Pd, Cu, Ag, Au), most generally displaying some sort of antiferromagnetic ordering [4,6,7,12–20]. Because of the layered nature of their structure, high anisotropy of these properties is expected, as has been demonstrated for $REAgSb_2$ [16] and $CeMSb_2$ (M = Cu, Au, Ni) [19,20]. Recently, large positive magnetoresistance (>100%) has been observed in some $RENi_{1-x}Sb_2$ compounds [12].

In analogy to $LaZn_{0.52}Sb_2$, it may be expected that substitution of M with Cd should lead to compounds with the composition "$RECd_{0.5}Sb_2$", which would be isoelectronic with $REAgSb_2$ and allow for a comparison for how the presence of defects influences the physical properties. In the $RECd_{1-x}Sb_2$ series (RE = La, Ce, Pr, Nd, Sm), single-crystal X-ray diffraction studies have established that the

*Corresponding author. Fax: +1 780 492 8231.
E-mail address: arthur.mar@ualberta.ca (A. Mar).

0022-4596/$ - see front matter © 2006 Elsevier Inc. All rights reserved.
doi:10.1016/j.jssc.2006.01.071

first two members actually have the compositions $LaCd_{0.700(5)}Sb_2$ [8] and $CeCd_{0.660(4)}Sb_2$ [21]. Only cell parameters refined from powder X-ray diffraction data are available for the remaining members [7,8], so it is not obvious if the limiting composition "$RECd_{0.5}Sb_2$" can be reached through a change in *RE*. To clarify the compositions of these compounds and to investigate the influence of defects, we provide here complete crystallographic studies for the remaining members, and for the first time, we present the electrical and magnetic properties for all compounds in this series.

2. Experimental

Starting materials were powders of the rare-earth metals La, Ce, Pr, Nd, or Sm (99.9%, Alfa-Aesar or Cerac), Cd (99.999%, Cerac), and Sb (99.999%, Alfa-Aesar). The crystals used for structure determination were initially obtained from a reaction of *RE*, Cd, and Sb in a 1:1:2 molar ratio. The mixture of the elements was placed in an evacuated fused-silica tube, which was heated at 600 °C for 2 d, 1000 °C for 2 d, and then cooled to room temperature over 6 d. After the compositions of these compounds were established to be $RECd_{\sim 0.7}Sb_2$, samples for property measurements were prepared by reaction of *RE*, Cd, and Sb in a 1:0.7:2 molar ratio at 1000 °C for 3 d followed by cooling to 600 °C over 4 d and further annealing for 12*d*. Powder X-ray diffraction patterns of these samples, obtained on an Inel powder diffractometer equipped with a CPS 120 detector, were in good agreement with those calculated from the single-crystal data and confirmed that the samples were phase-pure.

Single-crystal intensity data for $RECd_{1-x}Sb_2$ (*RE* = Pr, Nd, Sm) were collected on a Bruker Platform/SMART 1000 CCD diffractometer at 22 °C using ω scans. Crystal data and further details of the data collection are given in Table 1. Calculations were carried out with use of the SHELXTL (version 6.12) package [22]. Face-indexed numerical absorption corrections were applied. The centrosymmetric space group *P*4/*nmm* was chosen and initial atomic positions were found by direct methods, confirming the expected $HfCuSi_2$-type structure. Partial occupancy of the Cd site (2*b*) was signalled by its significantly elevated displacement parameters compared to the other sites, which were well-behaved. Successive refinements were performed in which the occupancy of each site was allowed to vary independently. These refinements proceeded in a straightforward manner, and confirmed that partial occupancy was found only in the Cd site. Final values of the positional and displacement parameters are given in Table 2. Interatomic distances are listed in Table 3. Further data, in the form of a CIF, have been sent to Fachinformationszentrum Karlsruhe, Abt. PROKA, 76344 Eggenstein-Leopoldshafen, Germany, as supplementary material No. CSD-416248, 416249, 416250 and can be obtained by contacting FIZ (quoting the article details and the corresponding CSD numbers).

Silver plate-shaped crystals were selected for electrical resistivity measurements and confirmed to be the desired

Table 1
Crystallographic data for $RECd_{1-x}Sb_2$ (*RE* = Pr, Nd, Sm)

Formula	$PrCd_{0.665(3)}Sb_2$	$NdCd_{0.659(3)}Sb_2$	$SmCd_{0.648(3)}Sb_2$
Formula mass (amu)	458.59	461.92	466.91
Space group	*P*4/*nmm* (No. 129)	*P*4/*nmm* (No. 129)	*P*4/*nmm* (No. 129)
a (Å)	4.3592(3)	4.3456(4)	4.3185(4)
c (Å)	10.8619(7)	10.8372(9)	10.7843(11)
V (Å^3)	206.40(2)	204.65(3)	201.12(3)
Z	2	2	2
ρ_{calcd} (g cm^{-3})	7.379	7.496	7.710
Crystal dimensions (mm)	$0.17 \times 0.15 \times 0.04$	$0.11 \times 0.08 \times 0.03$	$0.08 \times 0.07 \times 0.03$
Radiation	Graphite monochromated Mo*K*α, $\lambda = 0.71073$ Å	Graphite monochromated Mo*K*α, $\lambda = 0.71073$ Å	Graphite monochromated Mo*K*α, $\lambda = 0.71073$ Å
μ(Mo*K*α) (cm^{-1})	276.73	286.91	308.34
Transmission factors	0.047–0.353	0.089–0.445	0.116–0.428
2θ limits	$3.74° \leqslant 2\theta(\text{Mo}K\alpha) \leqslant 65.88°$	$3.76° \leqslant 2\theta(\text{Mo}K\alpha) \leqslant 66.14°$	$3.78° \leqslant 2\theta(\text{Mo}K\alpha) \leqslant 66.24°$
Data collected	$-6 \leqslant h \leqslant 6$, $-6 \leqslant k \leqslant 6$, $-16 \leqslant l \leqslant 16$	$-6 \leqslant h \leqslant 6$, $-6 \leqslant k \leqslant 6$, $-16 \leqslant l \leqslant 16$	$-6 \leqslant h \leqslant 6$, $-6 \leqslant k \leqslant 6$, $-16 \leqslant l \leqslant 16$
No. of data collected	2672	2705	2661
No. of unique data, including $F_o^2 < 0$	275	276	271
No. of unique data, with $F_o^2 > 2\sigma(F_o^2)$	274	273	269
No. of variables	13	13	13
$R(F)$ for $F_o^2 > 2\sigma(F_o^2)$[a]	0.016	0.016	0.019
$R_w(F_o^2)$[b]	0.037	0.037	0.043
Goodness of fit	1.178	1.163	1.110
$(\Delta\rho)_{max}$, $(\Delta\rho)_{min}$ (e Å^{-3})	1.38, −1.99	1.11, −1.81	1.32, −2.05

[a] $R(F) = \sum ||F_o| - |F_c|| / \sum |F_o|$.
[b] $R_w(F_o^2) = [\sum[w(F_o^2 - F_c^2)^2] / \sum wF_o^4]^{1/2}$; $w^{-1} = [\sigma^2(F_o^2) + (Ap)^2 + Bp]$ where $p = [\max(F_o^2, 0) + 2F_c^2]/3$.

Table 2
Atomic coordinates and equivalent isotropic displacement parameters for $RECd_{1-x}Sb_2$ (RE = Pr, Nd, Sm)

Atom	Wyckoff position	x	y	z	U_{eq} (Å^2)[a]
$PrCd_{0.665(3)}Sb_2$					
Pr	2*c*	1/4	1/4	0.22691(4)	0.00887(12)
Cd	2*b*	3/4	1/4	1/2	0.0263(3)
Sb1	2*a*	3/4	1/4	0	0.00922(13)
Sb2	2*c*	1/4	1/4	0.67629(5)	0.01102(13)
$NdCd_{0.659(3)}Sb_2$					
Nd	2*c*	1/4	1/4	0.22624(3)	0.00824(12)
Cd	2*b*	3/4	1/4	1/2	0.0253(3)
Sb1	2*a*	3/4	1/4	0	0.00839(12)
Sb2	2*c*	1/4	1/4	0.67746(5)	0.01021(13)
$SmCd_{0.648(3)}Sb_2$					
Sm	2*c*	1/4	1/4	0.22510(4)	0.00902(14)
Cd	2*b*	3/4	1/4	1/2	0.0251(4)
Sb1	2*a*	3/4	1/4	0	0.00867(15)
Sb2	2*c*	1/4	1/4	0.67968(6)	0.01054(15)

[a] U_{eq} is defined as one-third of the trace of the orthogonalized U_{ij} tensor.

Table 3
Selected interatomic distances (Å) for $RECd_{1-x}Sb_2$ (RE = La, Ce, Pr, Nd, Sm)

	$LaCd_{0.700(5)}Sb_2$	$CeCd_{0.660(4)}Sb_2$	$PrCd_{0.665(3)}Sb_2$	$NdCd_{0.659(3)}Sb_2$	$SmCd_{0.648(3)}Sb_2$
RE–Sb2 (× 4)	3.299(2)	3.2752(3)	3.2568(3)	3.2452(3)	3.2216(4)
RE–Sb1 (× 4)	3.339(2)	3.3095(4)	3.2902(3)	3.2760(3)	3.2489(4)
RE–Cd (× 4)	3.710(2)	3.6908(4)	3.6809(4)	3.6774(4)	3.6676(4)
Cd–Sb2 (× 4)	2.898(2)	2.9013(4)	2.9013(4)	2.9017(4)	2.9013(5)
Cd–Cd (× 4)	3.111(2)	3.0963(2)	3.0824(2)	3.0728(3)	3.0536(3)
Sb1–Sb1 (× 4)	3.111(2)	3.0963(2)	3.0824(2)	3.0728(3)	3.0536(3)
Reference	[8]	[21]	This work	This work	This work

ternary compounds by energy-dispersive X-ray (EDX) analysis with use of a Hitachi S-2700 scanning electron microscope. The electrical resistivity within the *ab* plane (ρ_{ab}) was measured by standard four-probe techniques on a Quantum Design PPMS system equipped with an ac transport controller (Model 7100). For $LaCd_{1-x}Sb_2$ and $CeCd_{1-x}Sb_2$, we were also able to measure the *c*-axis resistivity (ρ_c), but the values obtained should only be considered as estimates. The current was 100 μA and the frequency was 16 Hz. Magnetic susceptibility measurements were made on ground samples (~100 mg) on a Quantum Design 9T-PPMS dc magnetometer/ac susceptometer. The susceptibility was corrected for contributions for the holder diamagnetism and the underlying sample diamagnetism.

3. Results and discussion

As shown in Fig. 1, the $RECd_{1-x}Sb_2$ (RE = La, Ce, Pr, Nd, Sm) compounds adopt the $HfCuSi_2$-type structure, one of the most prevalent structure types among intermetallics. The structure consists of layers of condensed $CdSb_4$ tetrahedra separated from square Sb nets by the *RE* atoms. The square antiprismatic coordination of the *RE* atoms by the surrounding Sb atoms generally causes most of the other distances to decrease on progressing from $LaCd_{0.700(5)}Sb_2$ to $SmCd_{0.648(3)}Sb_2$, as expected from the lanthanide contraction. However, the Cd–Sb distances remain essentially invariant at ~2.90 Å, while the $CdSb_4$ tetrahedra become increasingly distorted, with the Sb–Cd–Sb angles changing from 115.1° (× 4) and 98.7° (× 2) in $LaCd_{0.700(5)}Sb_2$ to 116.5° (× 4) and 96.2° (× 2) in $SmCd_{0.648(3)}Sb_2$.

Partial occupancy of the *M* site is a common occurrence in $REM_{1-x}Sb_2$ compounds, and since it has been implicated from analysis on both powder and single-crystal samples, it appears to be an intrinsic phenomenon. The refined composition of the $RECd_{1-x}Sb_2$ compounds corresponds to a relatively constant (independent of *RE*) partial occupancy of the Cd site, at 0.65–0.66 for all members except for $LaCd_{0.700(5)}Sb_2$, which was annealed at a slightly different temperature (800 °C) [8]. As seen in the Cd–Sb distances, discussed above, size effects are likely not an important factor for controlling the degree of

non-stoichiometry. It seems clear that the formula $RECd_{\sim 0.7}Sb_2$ represents an upper limit for the Cd occupancy, since, as in most other syntheses of $REM_{1-x}Sb_2$ compounds reported in the literature, all these structure determinations were performed on crystals prepared from a 1:1:2 molar ratio of *RE*:Cd:Sb, that is, in the presence of an excess of Cd. The lower limit has not been determined, but this would be worthwhile investigating in a future study. Where homogeneity ranges have been determined, these have been fairly narrow, as in $LaMn_{0.65-0.76}Sb_2$ or $LaCu_{0.82-0.87}Sb_2$ [2], and a similar case may be expected for $RECd_{1-x}Sb_2$.

Conventionally, the bonding in these compounds has been rationalized by assuming that each Sb1 atom within the square net participates in four one-electron Sb–Sb bonds, yielding a formal charge of Sb^{1-}, whereas each isolated Sb2 atom has a formal charge of Sb^{3-} [23]. The partial occupancy can thus be understood through the formulation $(RE^{3+})(Cd^{2+})_{0.5}(Sb1)^{1-}(Sb2)^{3-}$. The observed Cd occupancy is closer to 0.65, but this is readily reconciled if the Sb1 atoms are considered to be reduced slightly further, to give $(RE^{3+})(Cd^{2+})_{0.65}(Sb1)^{1.3-}(Sb2)^{3-}$. As discussed elsewhere, the charge of the Sb1 atoms in the square net need not be integral, corresponding to a fractional filling of bands that are non-bonding or only weakly Sb–Sb antibonding in character such that no significant distortion of the Sb–Sb bonds takes place [23]. With the availability of more sophisticated treatments of electronic structure, it may be feasible to verify the electron count in $RECd_{1-x}Sb_2$ and related compounds through, for example, examination of the electron localization function [24].

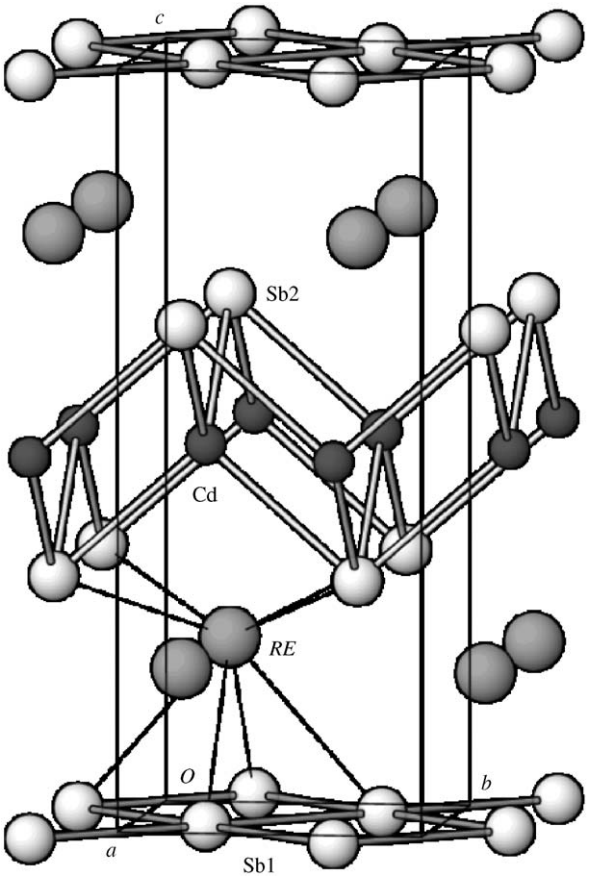

Fig. 1. Structure of $RECd_{1-x}Sb_2$, viewed approximately down the *a*-axis.

Table 4 summarizes the electrical and magnetic properties of $RECd_{0.7}Sb_2$ (*RE* = La, Ce, Pr, Nd, Sm), on samples that are assumed to have the maximum Cd content. Plots of the electrical resistivity within the *ab* plane (ρ_{ab}) are shown in Fig. 2. Except for the Ce phase, all $RECd_{0.7}Sb_2$ compounds appear to behave as normal metals, with a general trend towards decreasing resistivity on progressing from the La to the Sm phase. The residual resistivity ratios (RRR), which are a measure of the degree of perfection in a crystal, are substantially lower in the nonstoichiometric $RECd_{0.7}Sb_2$ compounds compared to the corresponding fully stoichiometric $REAgSb_2$ compounds [16], consistent with the enhanced scattering arising from defects. For $LaCd_{0.7}Sb_2$ and $CeCd_{0.7}Sb_2$, it was possible to measure not only the in-plane (ρ_{ab}), but also the *c*-axis (ρ_c) resistivity, shown in Figs. 2a and b, respectively. In both cases, ρ_c exceeds ρ_{ab} by one to two orders of magnitude, and the RRR values are lower in the *c* direction than in the *ab* plane, confirming the high anisotropy expected for these layered compounds. A TB-LMTO electronic structure calculation performed on $LaAgSb_2$ revealed that the Fermi level is crossed by two relatively wide bands between Γ and *X* (within the *ab* plane) but by a very narrow band (~0.3 eV in dispersion) between Γ and *Z* (along *c*) [17]. This feature explains the high anisotropy observed in $LaCd_{0.7}Sb_2$, assuming that it has a similar electronic structure as for $LaAgSb_2$ (with a band filling greater by only 0.4 e^- per formula unit). However, the role of defects, which are not easily modeled in a band structure calculation, must also be important.

Table 4
Physical properties of $RECd_{1-x}Sb_2$ (*RE* = La, Ce, Pr, Nd, Sm)

Compound	$\rho_{ab,\ 300}$ (μΩ cm)	χ_o (emu/mol)	θ_p (K)	$\mu_{eff,\ meas}$ (μ_B)	$\mu_{eff,\ theor}$ (μ_B)
$LaCd_{0.7}Sb_2$	48	4.7×10^{-4} (TIP)			
$CeCd_{0.7}Sb_2$	200	1.0×10^{-3}	−3.0	1.85	2.54
$PrCd_{0.7}Sb_2$	14	1.2×10^{-3}	−5.0	3.38	3.58
$NdCd_{0.7}Sb_2$	10	1.6×10^{-3}	−15.0	3.41	3.62
$SmCd_{0.7}Sb_2$	7.4	1.4×10^{-3}			

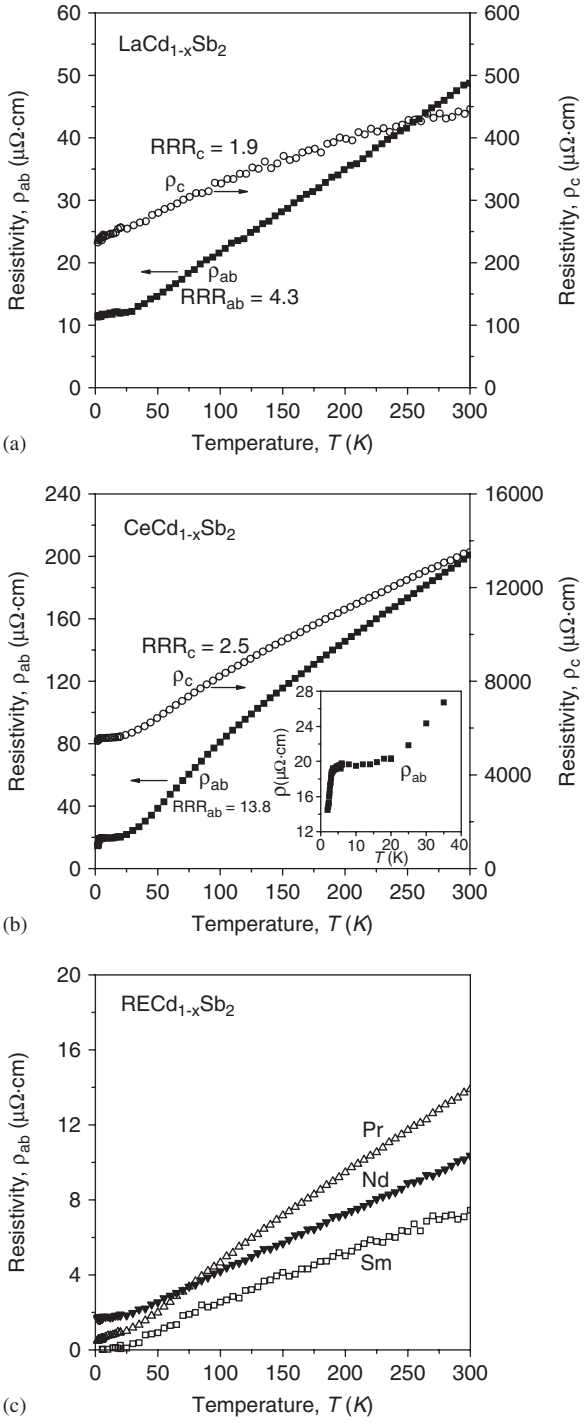

Fig. 2. Electrical resistivity of single crystals of $RECd_{1-x}Sb_2$ measured within the *ab* plane and parallel to *c* for (a) $RE = La$ and (b) $RE = Ce$, and measured within the *ab* plane for (c) $RE = Pr$, Nd, Sm. The inset in (b) shows the low-temperature behaviour in ρ_{ab} for $RE = Ce$.

With decreasing temperature, the in-plane resistivity (ρ_{ab}) of $CeCd_{0.7}Sb_2$ decreases and reaches a shallow minimum near 10 K, before undergoing an abrupt drop below ~3 K, as shown more clearly in the inset of Fig. 2b. The profile of this resistivity curve resembles that of other Ce-containing antimonides such as $CeNiSb_3$ [25,26] or $CeSn_{0.7}Sb_2$ [27], where Kondo-like behaviour has been suggested. Correspondingly, the temperature dependence of the dc magnetic susceptibility for $CeCd_{0.7}Sb_2$, shown in Fig. 3a, undergoes an abrupt increase at low temperatures. A T_C of 2.8 K was located from transitions observed in the real and imaginary components of the ac magnetic susceptibility curves (not shown). A fit of the inverse magnetic susceptibility to the modified Curie–Weiss law above 20 K leads to a slightly negative value of −3.0 K for θ_p, implying dominant antiferromagnetic coupling interactions between the Ce atoms, and an effective moment of 1.85 μ_B, which is smaller than the free-ion value for Ce^{3+}. The isothermal magnetization at 2 K, shown in Fig. 3b, exhibits saturation behaviour with little hysteresis. These observations are consistent with ferromagnetic ordering, but detailed understanding of the magnetic structure will require further study. In particular, it will be interesting to study the magnetization as a function of orientation, when larger single crystals become available.

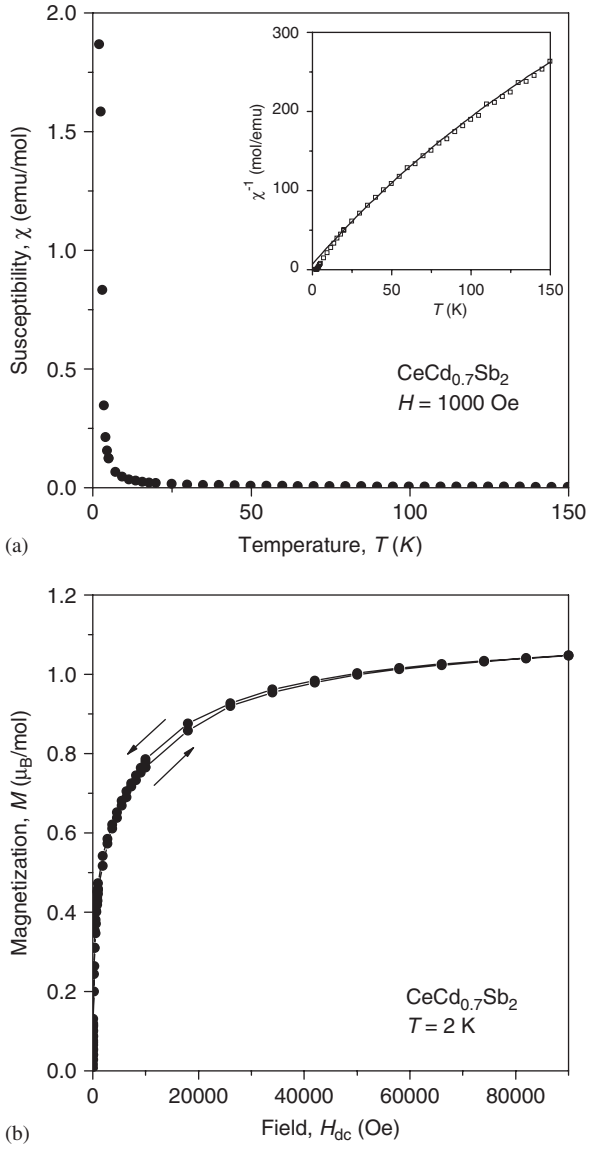

Fig. 3. $CeCd_{0.7}Sb_2$. (a) Magnetic susceptibility and its inverse (inset). (b) Isothermal magnetization at 2 K.

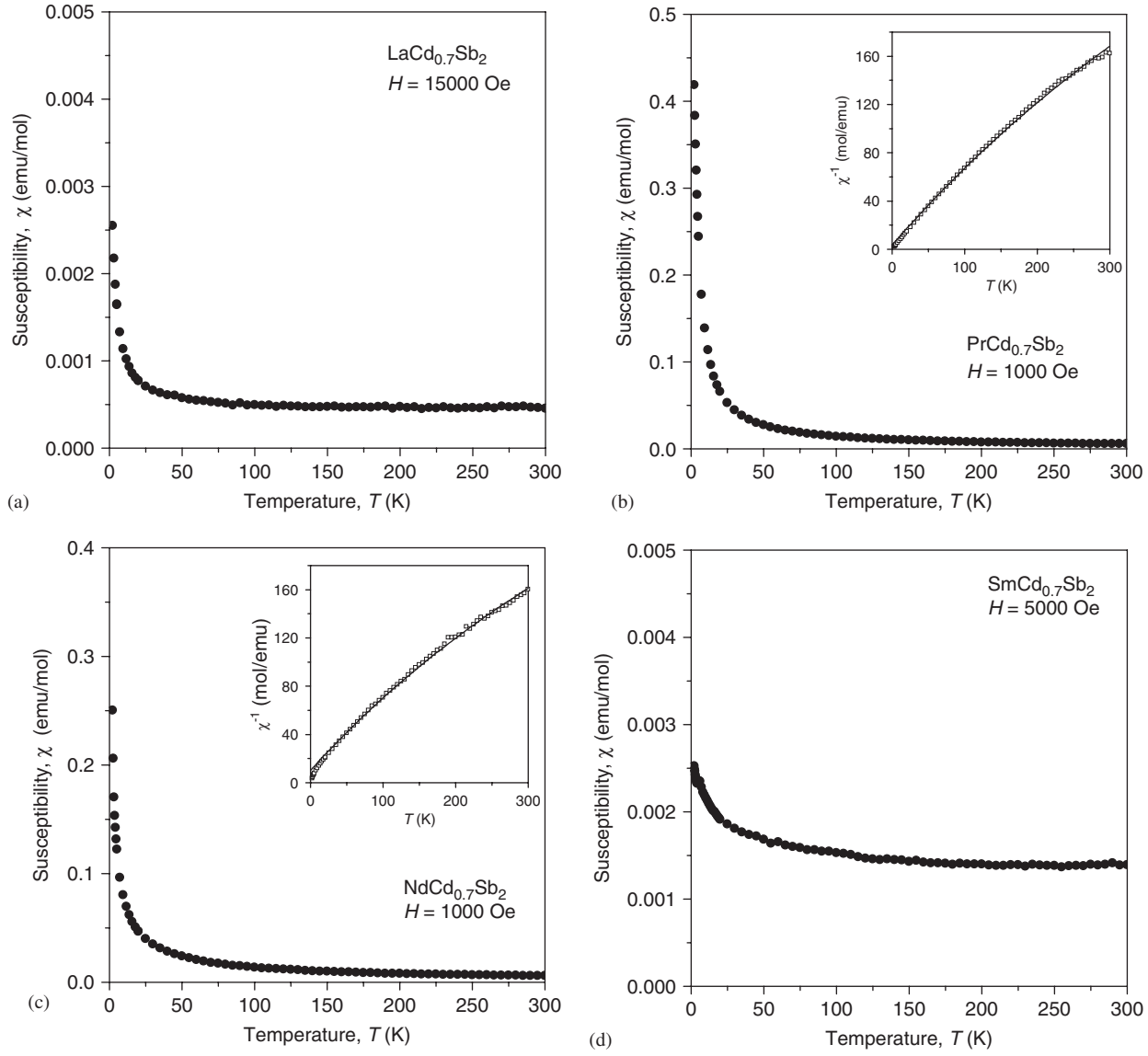

Fig. 4. Magnetic suspectibility for (a) $LaCd_{0.7}Sb_2$, (b) $PrCd_{0.7}Sb_2$, (c) $NdCd_{0.7}Sb_2$, and (d) $SmCd_{0.7}Sb_2$. The insets in (b) and (c) show the inverse susceptibility and fits to the modified Curie–Weiss law.

None of the remaining compounds displays any obvious magnetic ordering (Fig. 4). $LaCd_{0.7}Sb_2$ exhibits temperature-independent Pauli paramagnetism with a weak Curie tail at low temperatures arising from paramagnetic impurities (Fig. 4a). For $PrCd_{0.7}Sb_2$ and $NdCd_{0.7}Sb_2$ (Figs. 4b and c), fits of the inverse magnetic susceptibility to the modified Curie–Weiss law above 10 K lead to the parameters given in Table 4. The values of θ_p are negative, consistent with antiferromagnetic coupling, and the values of the temperature-independent term, χ_o, are relatively large, consistent with the metallic conductivity of these compounds. The effective moments in both cases are slightly smaller than the free-ion values for RE^{3+}. Typical of other Sm-containing intermetallics, $SmCd_{0.7}Sb_2$ does not follow Curie–Weiss behaviour (Fig. 4d) but displays van Vleck paramagnetism instead.

Acknowledgments

The Natural Sciences and Engineering Research Council of Canada and the University of Alberta supported this work. We thank Dr. Robert McDonald and Dr. Michael J. Ferguson (X-ray Crystallography Laboratory) for the X-ray data collection and Ms. Christina Barker (Department of Chemical and Materials Engineering) for assistance with the EDX analysis.

References

[1] Yu.V. Pankevich, V.K. Pecharskii, O.I. Bodak, Izv. Akad. Nauk SSSR Met. (1983) 227–229.
[2] G. Cordier, H. Schäfer, P. Woll, Z. Naturforsch. B: Anorg. Chem. Org. Chem. 40 (1985) 1097–1099.

[3] A. Leithe-Jasper, P. Rogl, J. Alloys Compd. 203 (1994) 133–136.
[4] O. Sologub, K. Hiebl, P. Rogl, H. Noël, O. Bodak, J. Alloys Compd. 210 (1994) 153–157.
[5] M. Brylak, M.H. Möller, W. Jeitschko, J. Solid State Chem. 115 (1995) 305–308.
[6] O. Sologub, H. Noël, A. Leithe-Jasper, P. Rogl, O.I. Bodak, J. Solid State Chem. 115 (1995) 441–446.
[7] O. Sologub, K. Hiebl, P. Rogl, O. Bodak, J. Alloys Compd. 227 (1995) 40–43.
[8] P. Wollesen, W. Jeitschko, M. Brylak, L. Dietrich, J. Alloys Compd. 245 (1996) L5–L8.
[9] Ł. Gondek, B. Penc, A. Szytuła, N. Stusser, J. Alloys Compd. 346 (2002) 80–83.
[10] L. Zeng, X. Xie, H.F. Franzen, J. Alloys Compd. 343 (2002) 122–124.
[11] L.P. Salamakha, S.I. Mudryi, J. Alloys Compd. 359 (2003) 139–142.
[12] E.L. Thomas, M. Moldovan, D.P. Young, J.Y. Chan, Chem. Mater. 17 (2005) 5810–5816.
[13] M. Houshiar, D.T. Adroja, B.D. Rainford, J. Magn. Magn. Mater. 140–144 (1995) 1231–1232.
[14] Y. Muro, N. Takeda, M. Ishikawa, J. Alloys Compd. 257 (1997) 23–29.
[15] M. Kolenda, M. Hofmann, J. Leciejewicz, B. Penc, A. Szytuła, A. Zygmunt, J. Alloys Compd. 315 (2001) 22–27.
[16] K.D. Myers, S.L. Bud'ko, I.R. Fisher, Z. Islam, H. Kleinke, A.H. Lacerda, P.C. Canfield, J. Magn. Magn. Mater. 205 (1999) 27–52.
[17] K.D. Myers, S.L. Bud'ko, V.P. Antropov, B.N. Harmon, P.C. Canfield, A.H. Lacerda, Phys. Rev. B 60 (1999) 13371–13379.
[18] C. Song, J. Park, J. Koo, K.-B. Lee, J.Y. Rhee, S.L. Bud'ko, P.C. Canfield, B.N. Harmon, A.I. Goldman, Phys. Rev. B 68 (2003) 035113-1–035113-6.
[19] A. Thamizhavel, T. Okubo, M. Yamada, A. Galatanu, E. Yamamoto, Y. Inada, T. Ebihara, Y. Ōnuki, Physica B 327 (2003) 374–377.
[20] A. Thamizhavel, T. Takeuchi, T. Okubo, M. Yamada, R. Asai, S. Kirita, A. Galatanu, E. Yamamoto, T. Ebihara, Y. Inada, R. Settai, Y. Ōnuki, Phys. Rev. B 68 (2003) 054427-1–054427-8.
[21] A.V. Tkachuk, A. Mar, Acta Cryst. E 60 (2004) i82–i83.
[22] G.M. Sheldrick, SHELXTL, Version 6.12, Bruker AXS Inc., Madison, WI, 2001.
[23] G.A. Papoian, R. Hoffmann, Angew. Chem. Int. Ed. 39 (2000) 2408–2448.
[24] A. Savin, O. Jepsen, J. Flad, O.K. Andersen, H. Preuss, H.G. von Schnering, Angew. Chem. Int. Ed. Engl. 31 (1992) 187–188.
[25] R.T. Macaluso, D.M. Wells, R.E. Sykora, T.E. Albrecht-Schmitt, A. Mar, S. Nakatsuji, H. Lee, Z. Fisk, J.Y. Chan, J. Solid State Chem. 177 (2004) 293–298.
[26] V.A. Sidorov, E.D. Bauer, H. Lee, S. Nakatsuji, J.D. Thompson, Z. Fisk, Phys. Rev. B 71 (2005) 094221-1–094221-4.
[27] L. Deakin, M.J. Ferguson, M.J. Sprague, A. Mar, R.D. Sharma, C.H.W. Jones, J. Solid State Chem. 164 (2002) 292–300.